Analysis of Visco-elastic-plastic Behaviour of Short Glass Fiber-reinforced Polyamide 66 Composite (PA66 GF30)

FELICIA STAN*, ANA VERONICA MUNTEANU, CATALIN FETECAU
Dunarea de Jos University of Galati, Faculty of Mechanical Engineering, 111 Domneasca Str., 800 211, Galati, Romania

In this paper, the behaviour of polyamide 66 with 30% short glass fibers (PA66 GF30) is investigated using instrumented indentation technique combined with the dynamic mechanical analysis (DMA). The visco-elastic-plastic behaviour of PA66 GF30 is described by a rheological model which incorporates a spring, a plastic element and Kelvin-Voigt elements. The time-temperature superposition (TTS) principle was used to investigate the effect of time and temperature on the behaviour of PA66 GF30.

Keywords: indentation, polyamide 66, creep, dynamic mechanical analysis

Polymeric materials exhibit visco-elastic behaviour which means that they simultaneously possess both solid-like and liquid-like characteristics. The visco-elastic behaviour of polymeric materials can be analyzed using different techniques such as instrumented indentation and dynamic mechanical analysis (DMA).

In the last years, indentation techniques have become the most popular method for studying the mechanical properties of polymeric materials whose response to load is time-dependent even at low temperature. The instrumented indentation method was initially developed to measure the hardness and elastic modulus of a material from indentation load-displacement data obtained during one cycle of loading and unloading [1]. In the last years, instrumented indentation methods were used to describe the visco-elastic-plastic behaviour of polymeric materials [2-4]. During the indentation, the variation of the indentation load as a function of indentation depth is continuously recorded. By a simple indentation test, Young's modulus, hardness, strain hardening exponent, fracture toughness and viscoelastic properties can be extracted.

Dynamic mechanical analysis (DMA) is a technique where a small deformation is applied to a sample in a cyclic manner. This allows the materials response to stress, temperature, frequency and other values to be studied. DMA data are used to obtain information about the storage and loss modulus, respectively.

In this paper, the visco-elastic properties of the polyamide 66 with short glass fibers are characterized by storage and loss modulus while the response of the material to constant load is described by creep indentation. The indentation creep is investigated based on a hereditary integral and on a rheological model which describes a full range of visco-elastic-plastic responses. The superposition principle is used to investigate the effect of time and temperature on the behaviour of PA66 GF30.

Instrumented indentation

Load–displacement curve

Figure 1 shows a typical load–displacement curve obtained during the indentation test. The load applied on the indenter is increased during the loading stage, kept constant at its maximum value during the holding stage (creep), and decreased to zero linearly during the unloading stage [1, 2].

The loading function used in the indentation test has the form:

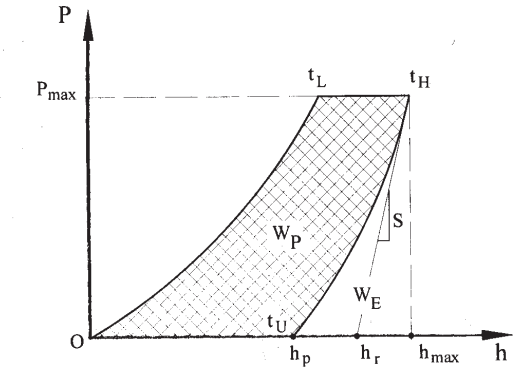

Fig. 1. Load–displacement curve for indentation

$$P(t)=\begin{cases} P_{\max}\dfrac{t}{t_L} & 0\le t\le t_L; \\ P_{\max} & T_L<t\le t_L+t_H; \\ P_{\max}\left(1-\dfrac{t}{t_U}\right) & t_L+t_H<t\le t_L+t_H+t_U, \end{cases} \quad (1)$$

where t_L, t_H, t_U are loading, holding and unloading time, respectively.

The loading part of the indentation curve generally follows Kick's law which can be expressed as [1, 2]

$$P=C\cdot h^2, \quad (2)$$

where P represents the indentation load, h is the penetration depth measured from the surface, and C is the compliance, the curvature of the loading curve which is a measure of the resistance of the material to indentation.

The contact geometry of a Vickers indenter with a specimen material is shown in figure 2, where α is the half included angle of the indenter, a_c and h_c are the contact radius and depth, respectively. For a Vickers indenter, the semi-angle α is 68° (the angle between the opposite planes of the Vickers pyramid is 136), thus the effective cone angle is 70.3°.

The maximum depth is reached under the maximal applied load. Due to plastic deformations some residual indentation depth (displacement) h_r remains after unloading.

* *email: felicia.stan@ugal.ro*

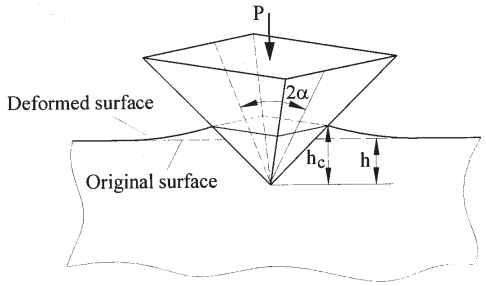

Fig. 2. Geometry of pyramidal indentation

For pyramidal indenters, such as Vickers, the contact radius can be deduced from the contact indentation depth, h_c, as follows:

$$a_c = h_c \tan\alpha_{eff} . \quad (3)$$

The initial unloading slope (or the contact stiffness) is defined as:

$$S = \left.\frac{dP_u}{dh}\right|_{h=h_{\max}}, \quad (4)$$

where P_u is the unloading force.

The compliance C corresponds to the inverse of the contact stiffness at the maximum indentation depth:

$$C = \frac{1}{S} = \left(\frac{dh}{dP}\right)_{h=h\max} \quad (5)$$

Due to the gradual reduction of contact area caused by elastic recovery, the unloading part of the P - h curve is nonlinear. Thus, the upper part of this curve can be fitted by a power law relation in the form [1, 4]

$$P = K(h - h_r)^m , \quad (6)$$

in which h_r corresponds to the final depth of the permanent imprint after unloading, i.e. the residual indentation depth, m and K are the fitting parameters.

The unloading slope can be then evaluated by differentiating equation (6) with respect to h

$$S = m \cdot K\left(h_{\max} - h_r\right)^{m-1} . \quad (7)$$

From the experimentally determined load-displacement data, the indentation hardness (H_{IT}) is evaluated by [2]

$$H_{IT} = \frac{P_{\max}}{A_p}, \quad (8)$$

where P_{max} is maximum indentation load, A_p is the projected (or cross-section) contact area at the maximum load.

The projected contact area for Vickers indenters with linear relationships between penetration depth and contact can be expressed as [5, 6]

$$A_p = k \cdot h_c^2 , \quad (9)$$

where k is a constant for a particular material and an indenter geometry.

The indentation modulus E_{IT} is obtained taking into account the elastic properties of the indenter (E_1, ν_1) and the Poisson ratio of the indented material, ν_s, as follows [6, 7]

$$E_{IT} = \frac{1-\nu_S^2}{\frac{1}{E_R} - \frac{1-\nu_I^2}{E_I}} . \quad (10)$$

in which the reduced modulus is given by

$$E_R = \frac{\sqrt{\pi}}{2\beta}\frac{S}{\sqrt{A_p}}, \quad (11)$$

where β is the geometrical correction factor for the indenter geometry. For the Vickers indenter, King [8] proposed a value β=1.012, whereas in [9] is proposed a value of 1.07.

If the diamond pyramid is assumed to be incompressible, the depth h can be calculated as:

$$h = \frac{d\sqrt{2}}{4}\cot\alpha , \quad (12)$$

where d is the diagonal of the indentation imprint.

The Vickers diamond hardness can be calculated as:

$$H = \frac{2P}{d^2}\sin\alpha . \quad (13)$$

The loading and unloading curves P - h can also yield information about energies involved in the process, such as the total work of indentation W_T (area under the curve) the elastic work W_E, released during unloading, and the plastic or irrecoverable energy W_P, which characterize the energy dissipated during the indentation plus the energy of residual stress around the imprint.

The curvature of the loading curve (C), the gradient at initial part of the unloading curve (S), and the ratio of the plastic work done to total work done W_P / W_T are three independent quantities which can be obtained from a single load–displacement curve [4, 5, 10] and used to determine elastic–plastic properties of an indented material.

Creep behavior

Based on the Sneddon's solution for pyramidal indentation [10], the relation between indenter load and the indentation displacement, P-h, under monotonic loading for an elastic material can be expressed as [11, 12]

$$h^2 = \frac{\gamma^2}{\pi\tan\alpha}\frac{1-\nu}{G}P, \quad (14)$$

where G is the shear modulus, ν is the Poisson's ratio of the half-space, α is the semi-angle of the indenter tip or equivalent cone, γ is a constant relating the contact displacement to the total displacement. For a Vickers or conical indenters, $\gamma = \pi / 2$.

The visco-elastic response from the indentation test is characterized based on the method proposed in [11, 12] in which the visco-elastic problem is solved starting from the elastic solution and replacing the elastic constants with their corresponding integral operators. The hereditary integral gives the strain at any time as a function of past history of the heredity of the polymer.

For the indentation into a linear visco-elastic material, if the hereditary integral analysis is applied to Eq. (14) the following equation for the time-dependent indentation displacement is obtained [13, 14]

$$h^2(t) = \frac{\gamma^2}{\pi\tan\alpha}\int_0^t J(t-s)\left[\frac{dP(s)}{ds}\right]ds, \quad (15)$$

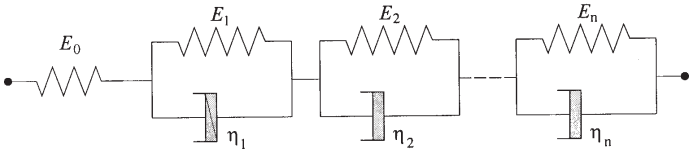

Fig. 3. Visco-elastic model

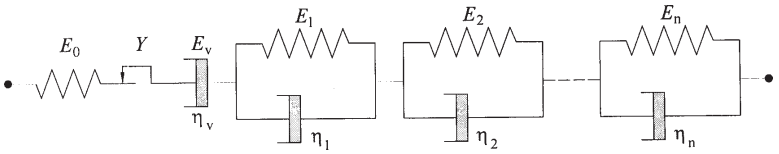

Fig. 4. Visco-elastic-plastic model

where s is the dummy variable for integration, t is the time, and $J(t)$ is the material creep compliance function. The hereditary integral (15) must be solved for the ramp loading and holding, respectively.

For indentation under constant load following ramp loading, eq. (15) leads to

$$h^2(t) = \frac{\gamma^2}{\pi \tan\alpha} k \int_0^{t_L} J(t-s)ds,\ t \geq t_L, \qquad (16)$$

where t_L is the time corresponding to the load increase (fig. 1), and $k=dP/dt$ is the loading rate. The solution of integral equation (16) is dependent on the creep function.

Visco-elastic solids with creep response can be modeled by a one-dimension model which consists of one spring and a series of Kelvin (Voigt) elements, figure 3. The creep function for the visco-elastic model in figure 3 can be expressed as

$$J(t) = C_0 + \sum_{i=1}^{n} C_i \left[1 - \exp\left(-\frac{t}{\tau_i}\right)\right] \qquad (17)$$

in which C_0 instantaneous elastic component, $\tau=\eta/E$ is the retardation time, C_i are the compliance constants.

After solving the hereditary integral (16) for the creep function (17), the following expression for the creep function during the holding period is obtained

$$h^2(t) = \chi k \left(C_0 t_L + t_L \sum_{i=1}^{n} C_i \left[1 - \exp\left(-\frac{t}{\tau_i}\right)\rho_i\right]\right), \qquad (18)$$

in which $\chi=\gamma^2$, $/(\pi\tan\alpha)$ and ρ_i represents the ramp correction factor defined by [13]:

$$\rho_i = \frac{\tau_i}{t_L}\left[\exp\left(\frac{t_L}{\tau_i}\right) - 1\right]. \qquad (19)$$

To incorporate the effect of plastic or visco-plastic deformations which occur beneath the sharp indenter, a visco-elastic-plastic model is considered [14, 15] as shown in figure 4. The rheological model incorporates a spring, a plastic element and Kelvin-Voigt elements. The instantaneous plastic deformation is characterized by a plastic element arranged in series with elastic element. The characteristic of the plastic element, Y, is incorporated in the compliance constant C_0. Moreover, the time-dependent irreversible viscous deformation is considered by introducing a dashpot of viscosity η_v in series with the visco-elastic model.

The resulting creep compliance function for the visco-elastic-plastic model is [15, 16]

$$J(t) = C_0 + C_v t + \sum_{i=1}^{n} C_i \left[1 - \exp\left(-\frac{t}{\tau_i}\right)\right], \qquad (20)$$

where C_i are constants and τ_i $(i=1,\ldots, n)$ is retardation time.

After solving the hereditary integral (16) for the creep function (20), the following expression for the creep function during the holding period is obtained [15, 16]

$$h^2(t) = \chi k \left(C_0 t_L + C_v t_L \left(t - \frac{t_L}{2}\right) + t_L \sum_{i=1}^{n} C_i \left[1 - \exp\left(-\frac{t}{\tau_i}\right)\rho_i\right]\right), \qquad (21)$$

Dynamic mechanical analysis

The visco-elasticity behaviour of polymeric materials can be also studied using the dynamic mechanical analysis. Figure 5 presents relationship between the stress and strain for polymeric materials. For perfect elastic materials, the stress and strain are in phase, while for perfect viscous materials the strain lags stress by a 90 degree. Visco-elastic materials exhibit properties in the middle of these two types of material.

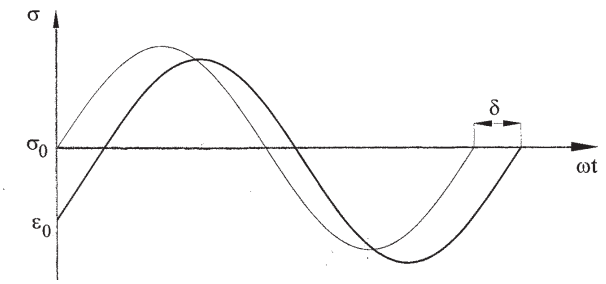

Fig. 5. Sinusoidal oscillation and response of a linear-viscoelastic material

The overall constitutive behaviour can be expressed in terms of the complex modulus [16, 17]

$$E^*(\omega) = E'(\omega) + \mathbf{i}E''(\omega) = \frac{\sigma}{\varepsilon}(\cos\delta + \mathbf{i}\sin\delta) \qquad (22)$$

where E' is the storage modulus (elastic response), E" is the loss modulus (viscous response).

The storage modulus and loss modulus of a polymeric material are measured as a function of temperature or time as the material is deformed under an oscillatory load at a controlled temperature.

An important quantity is the damping factor or loss tangent defined by [16, 17]

$$\tan\delta = \frac{E''(\omega)}{E'(\omega)}, \qquad (23)$$

and represents the amount of mechanical energy dissipated as heat during the loading/unloading cycle.

Another way to describe the visco-elastic behavior of polymeric materials is the time-temperature superposition (TTS) principle [16, 17]. Based on this principle, the relaxation modulus determined at temperature T and time $a_T t$ is equivalent to the relaxation modulus at reference temperature T_R and time t.

The amount of shifting along the horizontal axis in the TTS is described using one of two common theoretical models [16].

The first model is given by the Williams – Landel- Ferry (WLF) equation [16]

$$\log a_T = \frac{-C_1(T - T_R)}{C_2 + (T - T_R)} \quad (24)$$

where T_R is the reference temperature, C_1 and C_2 are parameters depending on material associated with fractional free volume and the empirical Doolittle expression.

Since above the glass transition temperature the fractional free volume increases linearly against temperature the WLF equation is used to describe the time/ temperature behaviour of polymers in the glass transition region.

The second model is the Arrhenius equation which describes the behaviour of a polymer outside the glass transition region. Based on the Arrhenius equation, the shift factor can be expressed as follows [16]:

$$\log a_T = \frac{E}{R}\left(\frac{1}{T} - \frac{1}{T_R}\right). \quad (25)$$

where E is the activation energy, R is the universal gas constant (=831 J/mol K), T is the measurement temperature, and T_R is the reference temperature. The activation energy can be determined from the slope of the curve of log a_T against 1 / T.

Material and methods

Material

The material under consideration is a polyamide 66 (PA66 GF30) filled with short glass fibre (30% by weight). Because of their mechanical properties at elevated temperature and thermal stability, polyamides are considered to be one of the most important engineering materials [18, 19].

The thermal properties were obtained by Differential Scanning Calorimetry. DSC analysis was carried out with a heating/cooling rate of 5°C min^{-1} in a temperature interval 25– 300°C and 10mg polyamide 66 sample. The melting peak temperature as determined from DSC measurements is about 260°C, while the glass transition temperature is about 60°C. The degradation temperature was determined using thermogravimetric analysis. The 10mg specimen was heated in the range of 20- 600°C with 10°C/min in nitrogen atmosphere. The temperature of thermal degradation (at weight loss of 2%) is 308°C, while the temperature of maximum thermal degradation is 458.5°C. The total loss mass percent W (%) is 69.17

Indentation test

Indentation test was conducted using a CSM Micro Indenter with a Vickers indenter (2α =138°). The indentation test was performed at room temperature for an applied load of 5000 mN, following ramp loading using a trapezoidal loading function [2]. The loading and unloading rates were identical (5000 mN/min), and the creep time (holding time, t_H) was 40 s. The trapezoidal loading function used in the indentation test is presented in figure 6.

The indentation P - h response is shown in figure 7. A creep like behaviour is observed when the load is maintained constant at the end of the loading phase (fig. 7). The third part of the indentation curve leads to elastic recovery of the material and its initial slope is used to derive the elastic indentation modulus. The indentation creep behaviour is shown in figure 8. In this figure, the creep displacement has been set to zero at the start of the holding period, t_L = 60s.

The tangent method was used to extract the tangent stiffness, S, and the contact area measured at the maximum indentation load (fig. 9). The indentation

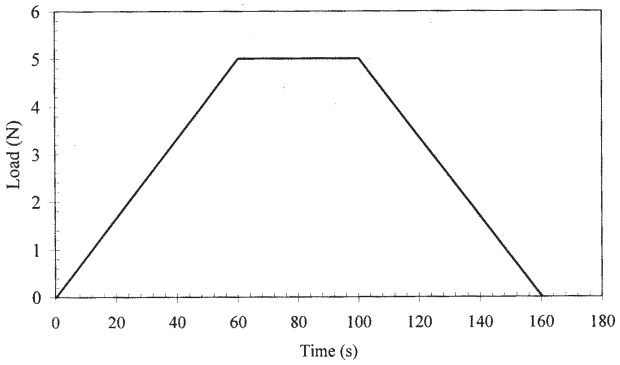

Fig. 6. Variation of load with time for indentation

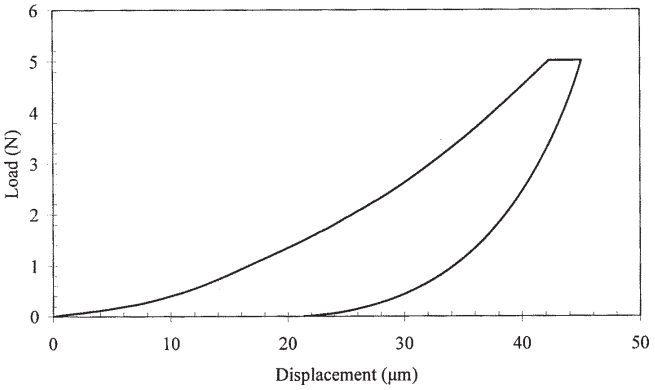

Fig. 7. The load-displacement curve for PA66 GF30 at 5 N

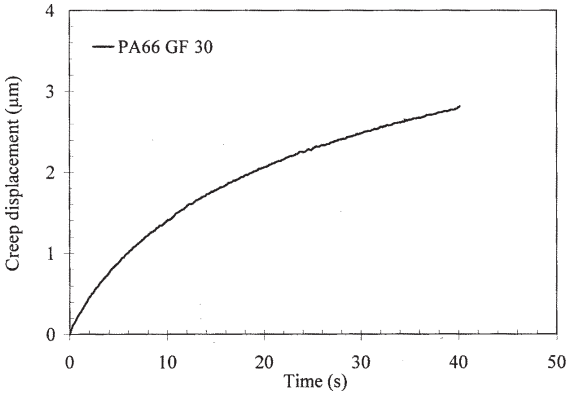

Fig. 8. Creep displacement – time responses for indentation experiment

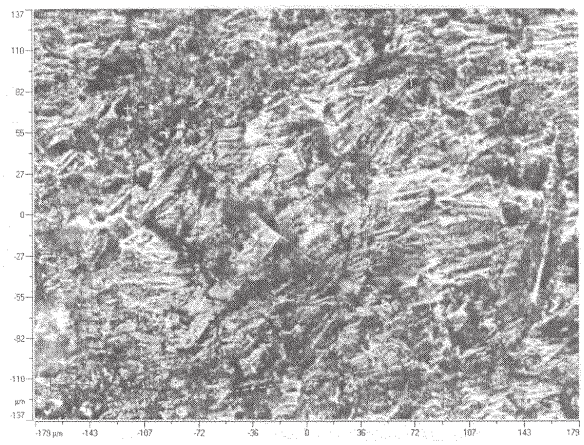

Fig. 9. The indentation cross-section area

hardness and indentation modulus were then calculated using equation (8) and (10), respectively. Based on the experimental results the elastic work, plastic work, and the elastic part of the indentation work η_{IT} were estimated. The main results extracted from the indentation tests are summarized in table 1.

Table 1
INDENTATION PARAMETERS

P_{max} (mN)	5000
h_{max} (μm)	45.04
h_p (μm)	21.37
h_r (μm)	37.66
h_c (μm)	39.51
t_L (sec)	60.17
t_H (sec)	100.12
t_U (sec)	160.29
E_r (GPa)	3.02
E_{IT} (GPa)	2.49
H_{IT} (MPa)	130.75
S (N/m)	674.51×10^3
W_{elast} (pJ)	31.65
W_{plast} (pJ)	57.59
η_{IT} (%)	35.47

test was performed on 2.34mm thick rectangular block having an area of 10mm×10mm.

The temperature scans were run from -30 to 200°C at a heating rate of 4C/min using multi frequency/single strain mode. A total of five frequencies (0.1, 0.316, 1, 3.16, and 10 Hz) were swept at each temperature.

For example, the DMA curve of PA66 GF30 measured at a frequency of 1 Hz is shown in figure 11. The peak in damping factor (tan delta) indicates the glass transition (T_g) temperature.

Figure 12 shows the storage modulus of the PA66 GF30 sample as a function of temperature for five different frequencies. The storage modulus (E') master curve shows how the stiffness of the polymeric material changes with frequency.

Table 2
BEST FIT PARAMETERS FOR PA66 GF 30

Model	C_0 (m^2/N)	C_1 (m^2/N)	C_2 (m^2/N)	C_v (m^2/Ns)	τ_1 (s)	τ_2 (s)	R^2
(i) S+KV	$22.85\ 10^{-12}$	$5.75\ 10^{-12}$	-	-	20.05	-	0.999
(ii) S+D+KV	$21.11\ 10^{-12}$	$6.13\ 10^{-12}$	-	$1.67\ 10^{-14}$	10.34	-	1.0
(ii) S+D+KV	$17.73\ 10^{-12}$	$4.23\ 10^{-12}$	$5.49\ 10^{-12}$	$1.41\ 10^{-14}$	1.64	12.33	0.999

R^2 – Goodness of fit

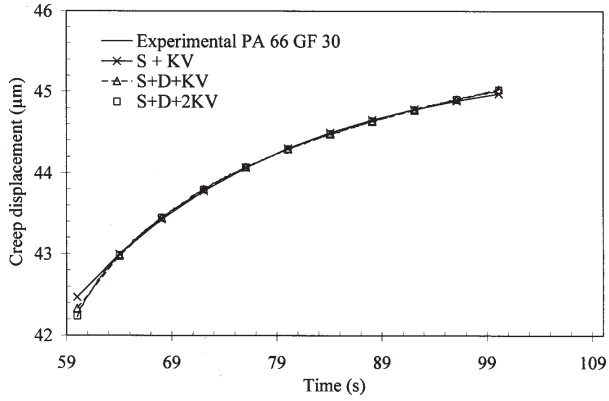

Fig. 10. Creep displacement – time response and fitted lines corresponding to rheological equations

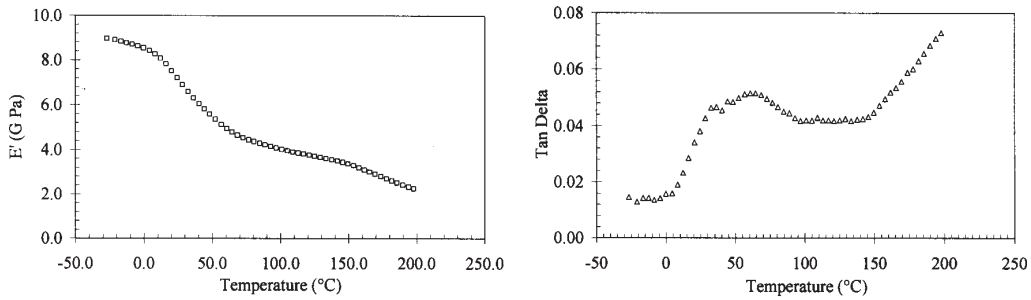

Fig. 11. DMA curves of PA66 GF30 frequency of 1 Hz: (a) storage modulus, (b) tan δ

(a) (b)

In order to investigate the creep response, the experimental creep data were fitted to different viscous model: (i) Spring and one Kelvin-Voigt body (S+KV), (ii) Spring, Dashpot and one Kelvin-Voigt body (S+D+KV), (iii) Spring, Dashpot and two Kelvin-Voigt bodies (S+D+2KV). The model parameters and the corresponding fitting errors are summarized in table 2.

Dynamic mechanical analysis (DMA) test

In order to investigate the time-dependent properties of PA66 GF30, the frequency–temperature dependent viscoelastic mechanical properties including storage (E'), loss modulus (E") and the mechanical loss factor (tan δ) were measured by dynamic mechanical analysis (DMA) using TA Instruments DMA Q800. A single cantilever beam

A frequency temperature master curve for the storage modulus was created. Each isotherm was shifted along the log frequency axis relative to a reference isotherm in order to achieve maximum overlap of the data (fig. 13). Generally, the reference temperature can be selected between glass transition temperature of polymer, and T_g+100°C [16, 17]. The reference temperature for the presented master curves is 60°C, corresponding to the softening temperature of the PA66 GF30 at 1 Hz frequency.

The corresponding shift factor plot is given in figure 14. The temperature-shift factor, $\log a_T$, represents the number of log (frequency) units through which an isotherm was translated. WLF constants were determined based on the equation (24).

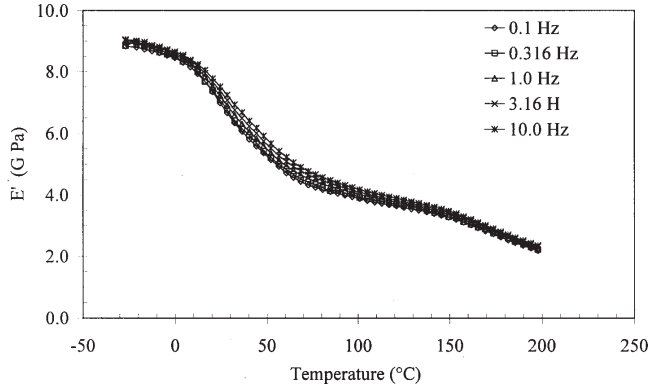

Fig. 12. Storage modulus of PA 66 GF30 versus temperature

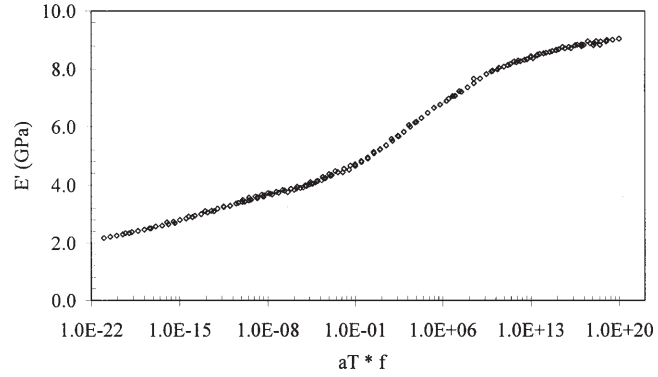

Fig. 13. Master curve of PA66 GF30, T_{ref}=60°C

Since figure 14 shows considerable change in the slope as the shift factor passes through the glass transition temperature, to improve the accuracy of shift factor, the shift factor was fitted separately both above and below the glass transition temperature as shown in table 3.

Conclusions

In this paper, the visco-elastic-plastic behaviour of polyamide 66 with 30% short glass fibers (PA66 GF30) was investigated using instrumented indentation technique and dynamical mechanical analysis (DMA), respectively. Experimental results from Vickers indentation creep tests of PA66 GF30 were analyzed using an analytical approach based on hereditary integral operator and visco-elastic-plastic model. The model fitted well to the experimental load–displacement from indentation experiment, indicating the capability of the model to reproduce the holding part of the load-displacement curve. The superposition principle was used to create a frequency temperature master curve based on the storage modulus curves, and the Williams–Landel–Ferry constants were determined. The model parameters obtained in this paper may be used as input data for finite element analysis.

Acknowledgements: This work was supported by CNCSIS –UEFISCSU, project number PNII – IDEI 788/2008.

Reference

1. W.C. OLIVER, G.M. PHARR, 1992, An improved technique for determining hardness and elastic modulus using load and displacement sensing indentation experiments, Journal of Materials Research, vol. 7, no. 6, p. 1564
2. A.C. FISCHER-CRIPPS, Nanoindentation, 2nd Ed, New York, Springer-Verlag, 2004
3. W.C., OLIVER, G. PHARR, 2004, Measurement of hardness and elastic modulus by instrumented indentation: Advances in understanding and refinements to methodology Journal of Materials Research, vol. 19, p. 3

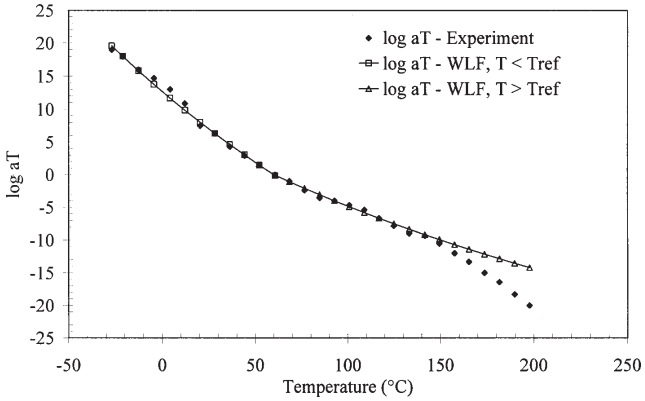

Fig. 14. The thermal shift factor

Table 3
WLF FITTING PARAMETERS WITH REFERENCE TEMPERATURE TO 60°C

Model	T_{ref} (°C)	C_1	C_2
$T > T_{ref}$	60	69.52	537.3
$T < T_{ref}$	60	93.78	503

4. M. VANDAMME, F.-J.Ulm, 2006, Viscoelastic solutions for conical indentation, International Journal of Solids and Structures, vol. 43, p. 3142
5. Z. SHI et al., 2010, The equivalent axisymmetric model for Berkovich indenters in power-law hardening materials, International Journal of Plasticity, vol. 26, p. 141
6. A.E. GIANNAKOPOULOS, P.L. LARSON, E. SODERLUND, D.J. ROWCLIFFE, R. VESTERGAARD, 1994, Analysis of Vickers indentation, International Journal of Solids and Structures, vol. 31, no. 19, p. 2679
7. *** CSM Instruments, 2006, Investigation of creep behavior using Micro or Nano Indentation Tester (MHT/NHT) APPLICATIONS BULLETIN, no. 22
8. KING, R.B., 1987, Elastic analysis of some punch problems for a layered medium, International Journal of Solids and Structures, vol. 23, no. 12, p. 1657
9. M. DAO, N. CHOLLACOOP, K. J. VAN VLIET, T. A. VENKATESH , S. SURESH, 2001, Computational modeling of the forward and reverse problems in instrumented sharp indentation, Acta Materialia, vol. 49, p. 3899
10. I.N. SNEDDON, 1965, The relation between load and penetration in the axisymmetric Boussinesq problem for a punch of arbitrary profile, International Journal Engineering and Science, vol. 3, p. 47
11. J.R.M. RADOK, 1957, Visco-elastic stress analysis Quarterly of Applied Mathematics, vol. 15, p. 198
12. E.H. LEE, J.R.M. RODOK, 1960, The contact problem for viscoelastic bodies, Journal of Applied Mechanics, vol. 27, p. 438
13. M.L. OYEN, 2006, Analytical techniques for indentation of viscoleastic materials, Philosophical Magazine, vol. 86, no. 33-35, p. 5625
14. R. SHAHSAVARI, F.J ULM, 2009, Indentation analysis of fractional viscoelastic solids, Journal of Mechanics of Materials and Structures, vol. 4, no. 3, p. 523
15.J. MENCIK, L.H. HE, M.V. SWAIN, 2009, Determination of viscoelastic-plastic material parameters of biomaterials by instrument indentation, Journal of the Mechanical Behavior of Biomedical Materials, vol. 2, p. 318
16. D.J. FERRY, Viscoelastic Properties of Polymers, Wiley; 3rd Edition, 1980
17. K.P. MENARD, Dynamic mechanical analysis: A practical introduction, CRC Press, 2008
18. GH. MARIES, I. MANOVICIU, G. BANDRU, G. RUSU, V. POPA, 2009, Study by Thermal Methods of some physico-mechanical properteis of polyamides used for high performance sport products, Materiale Plastice, vol. 46, no. 1, p. 58
19. JING-LEI YANG, ZHONG ZHANG, ALOIS K. SCHLARB, KLAUS FRIEDRICH, 2006, On the characterization of tensile creep resistance of polyamide 66 nanocomposites. Part II: Modeling and prediction of long-term performance, Polymer, vol. 47, p. 6745

Manuscript received: 4.10.2010